Solar Physics (2025) 300:133
https://doi.org/10.1007/s11207-025-02535-8

RESEARCH

Role of CME Clusters and CME-CME Interactions in Producing Sustained γ-Ray Emission Events

Atul Mohan[1,2] · **Pertti Mäkelä**[1,2] · **Natchimuthuk Gopalswamy**[1] · **Sachicko Akiyama**[1,2] · **Seiji Yashiro**[1,2]

Received: 1 April 2025 / Accepted: 14 August 2025

Abstract

Fast ($V_{CME} > 1000\ km\,s^{-1}$) coronal mass ejections (CMEs) capable of accelerating protons beyond 300 MeV are thought to trigger hours-long sustained γ-ray emission (SGRE) after the impulsive flare phase. Meanwhile, CME-CME interactions can cause enhanced proton acceleration, increasing the fluxes of solar energetic particles. This study explores the role of fast CME interactions in SGRE production during CME clusters, which we define as a series of CMEs linked to > C-class flares with waiting times < 1 day from the same active region (AR). We focus on clusters in major CME-productive ARs (major ARs), by defining a major AR as one that produced > 1 CME associated to a major (> M-class) flare. The study identified 76 major ARs between 2011 and 2019, of which 12 produced all SGRE events. SGRE-producing ARs exhibit higher median values for the speed of their fastest CMEs (2013 vs. 775 $km\,s^{-1}$) and the class of their strongest flares (X1.8 vs. M5.8), compared to SGRE-lacking ARs. They also produced relatively faster CMEs (median speed: 1418 vs. 1206.5 $km\,s^{-1}$), with the SGRE-associated CMEs occurring during periods of higher CME rates than typical fast CME epochs. Twelve of 22 (54.5%) SGRE events and 5 of 7 (71.4%) long-duration (> 10 h) SGRE events occurred during CME clusters, with high chances of CME-CME interactions. A case study on very active major ARs showed that all SGRE-associated CMEs with $V_{CME} \lesssim 2000\ km\,s^{-1}$ underwent CME-CME interactions within $\lesssim 10\ R_\odot$, while SGRE-associated CMEs faster than 3000 $km\,s^{-1}$ did not undergo interactions.

Keywords Coronal mass ejections, interplanetary · Energetic particles, acceleration · Energetic particles, protons · Radio bursts, type II

1. Introduction

A sustained γ-ray emission (SGRE) event is characterized by an extended period of enhanced γ-ray flux lasting up to several hours, beginning after the impulsive phase of the

✉ A. Mohan
atul.mohan@nasa.gov

P. Mäkelä
pertti.a.makela@nasa.gov

1 NASA Goddard Space Flight Center, 8800 Greenbelt Road, Greenbelt, MD, 20771, USA

2 The Catholic University of America, Washington, DC, USA

associated flare. SGRE events were first reported and demonstrated to be distinct from the impulsive flare-phase emission by Forrest et al. (1985) using data from the Gamma Ray Spectrometer (GRS; Forrest et al. 1980) on board the Solar Maximum Mission. Subsequent missions such as Gamma-1 (Akimov et al. 1991) and Energetic Gamma-Ray Experiment Telescope (Kanbach et al. 1989) enabled SGRE spectral observations up to a few GeV. Detailed modeling of various SGRE events highlighted the need for coronal shocks in accelerating protons above 300 MeV to produce the observed > 100 MeV spectrum (Murphy, Dermer, and Ramaty 1987; Akimov et al. 1992). The reported similarity between the spectra of an SGRE and the co-temporal solar energetic particle (SEP) events, likely accelerated by the same shock, is noteworthy (Forrest et al. 1985). However, the SGRE event sample size remained scarce until the advent of the Fermi-Large Area Telescope (Fermi/LAT; Atwood et al. 2009), which offered a superior sensitivity and a wider field of view, allowing extended periods of solar monitoring. The latest Fermi/LAT SGRE event catalog (Ajello et al. 2021) has 22 events with durations over 3 hours (> 3 h SGRE events). Various studies have demonstrated the association of > 3 h SGRE events with coronal mass ejection (CME) shocks using γ-ray to radio band data (e.g. Ackermann et al. 2017; Gopalswamy et al. 2018a; Pesce-Rollins et al. 2022; Mäkelä et al. 2023). The SGRE-associated CMEs resemble CMEs that accelerate protons beyond 100 MeV, causing ground-level enhancements, recorded by neutron monitors (Gopalswamy et al. 2018a)

Meanwhile, alternative SGRE models have been proposed. A major alternative model invokes large flare loops that trap and re-accelerate particles for hours post-flare (Ryan and Lee 1991; Mandzhavidze and Ramaty 1992; Hudson 2018; de Nolfo et al. 2019). However, sustaining post-flare proton acceleration for > 3 h imposes stringent conditions on the turbulence within the loops and extended particle acceleration episodes in the active regions (ARs), which are strongly debated (Ramaty and Mandzhavidze 1998; Kahler, Cliver, and Kazachenko 2018). For instance, Kanbach et al. (1993) attempted to explain the SGRE of 1991 June 11 that lasted more than 8 hours using a turbulent flare-loop model. The authors ended up demonstrating that only turbulence-free loops can efficiently trap the particles for so long, contradicting the fundamental framework of the model which requires turbulence to re-accelerate particles to energies > 300 MeV. Also, SGRE sources observed at $\approx 35°$ behind the limb will require unusually large loops to transport particles and cause precipitation on the front side. However, CME shocks that extend across large scales easily explain particle acceleration and magnetic connectivity to the SGRE source, as demonstrated in various events (Pesce-Rollins et al. 2015; Ackermann et al. 2017; Gopalswamy et al. 2020; Pesce-Rollins et al. 2022). Data-driven modeling of three behind-the-limb SGRE events by Plotnikov, Rouillard, and Share (2017) showed that, in each case, a CME shock producing a co-temporal SEP event could be associated with the SGRE. Gopalswamy et al. (2018b) reported a correlation between the durations of > 3 h SGRE events and the co-temporal decameter hectometric (DH) type II bursts driven by CME shocks, providing another strong support for the CME-shock association of SGRE events. The > 3 h SGRE events are generally associated with fast (> 1000 km s^{-1}) and wide (mostly halo) CMEs with relatively high initial accelerations (Mäkelä et al. 2023). The work presented here focuses on > 3 h SGRE events, due to their strong association with CMEs (Gopalswamy et al. 2019; Mäkelä et al. 2023).

Meanwhile, several studies have shown that CME-CME interactions during periods of successive CMEs with short waiting times, referred to as CME clusters (Ruzmaikin, Feynman, and Stoev 2011; Rodríguez Gómez et al. 2020a), are often associated with increased SEP fluxes and geomagnetic disturbances (Gopalswamy et al. 2004; Pomoell and Poedts 2018; Rodríguez Gómez et al. 2020b; Koehn et al. 2022; Mayank et al. 2024). Gopalswamy

et al. (2001c) discovered enhanced DH type II radio emission during a CME-CME interaction, signifying an increased particle acceleration efficiency. Later, various other groups also reported similar cases of enhancement in type II burst emission during CME-CME interaction events (e.g. Reiner et al. 2003; Martínez Oliveros et al. 2012; Ding et al. 2014; Temmer et al. 2014). Meanwhile, analyzing the CMEs and ARs associated with SGRE events, Gopalswamy et al. (2019) found that several events occurred during CME clusters hosted by some major CME-productive ARs (major ARs). CME-CME interactions in these clusters involving fast CMEs could have played a role in accelerating protons beyond 300 MeV, through mechanisms similar to those proposed to explain enhanced SEP fluxes (see, Lugaz et al. 2017, for a review). These $>$ 300 MeV protons could precipitate to deeper layers of the solar atmosphere, producing SGRE through various weak nuclear interactions (Ramaty et al. 1983; Murphy, Dermer, and Ramaty 1987). This work will define major ARs and CME clusters relevant in the context of SGRE events, systematically identify and characterize them using various parameters, and investigate the role of CME clusters and CME-CME interactions in SGRE production.

Section 2 introduces the data sources, methodology, and definitions used in this work. Section 3 presents the major AR catalog and compares the activity characteristics of SGRE-producing and SGRE-lacking major ARs. The section also discusses the properties of fast CMEs, their epochs, and their association with CME clusters. A case study on the role of CME-CME interactions in triggering SGRE events is also presented. Section 4 summarizes our conclusions.

2. Data and Methodology

The $>$ 3 h SGRE events in the Fermi/LAT event lists (Share et al. 2018; Ajello et al. 2021) and the CME database compiled by the Coordinated Data Analysis Workshop (CDAW) Data Center (CDAW CME catalog; Yashiro et al. 2004; Gopalswamy et al. 2009) form our main data source. Since we are interested only in strong CME-CME interactions capable of producing $>$ 300 MeV protons, the study is focused only on CMEs associated with $>$ C-class flares. The flare class is a metric of the peak soft X-ray (SXR) flare flux, which is an indicator of the strength of the reconnection event that propels the CME (Pevtsov et al. 2003; Kazachenko 2023; Mohan et al. 2024). The peak SXR flare flux therefore correlates with the CME speed (V_{CME}) observed in the Large Angle and Spectrometric Coronagraph (LARGE) C2 and C3 fields of view (Yashiro and Gopalswamy 2008; Salas-Matamoros and Klein 2015). Besides, interactions between CMEs associated with $>$ C-class flares have been shown to enhance SEP fluxes in $>$ 10 MeV bands (Gopalswamy et al. 2004, 2019). Meanwhile, since the Fermi/LAT SGRE event lists cover only Solar Cycle 24 starting from 2011, this study focuses on CMEs associated with $>$ C-class flares that occurred in major ARs between 2011 and 2019.

We define a major AR as an AR that produced more than one CME-associated major ($>$ M-class) flare in its observed lifetime. A catalog of AR sources of the CMEs associated with $>$ C-class flares during 2011 – 2019 was made using data from the CDAW CME catalog version 2.0 (Gopalswamy et al. 2024)[1] For each major AR, we cataloged every associated CME, noting the SXR flare strength (F_{CME}), V_{CME}, residual acceleration (a_{CME}), onset time, and duration, forming the primary database for this study. The CDAW CME catalog reports

[1] https://cdaw.gsfc.nasa.gov/CME_list/ The ARs that met the major AR criteria were then identified.

Table 1 Definitions of various terms used in this work related to CMEs associated with > C-class flares, ARs, CME occurrence periods and SGRE events.

Term	Definition
Fast CME	A CME with a sky-plane speed > 1000 km s^{-1}.
Very fast CME	A CME with a sky-plane speed > 1500 km s^{-1}.
SGRE-associated CME	A CME associated with an SGRE.
Major AR	An AR that produced more than one CME-associated major (> M-class) flare during its observed lifetime.
Major activity period	The period between the first and the last observed CMEs associated with > C-class flares.
SGRE-producing AR	An AR that produced ≥ 1 SGRE event in its observed lifetime.
SGRE-lacking AR	An AR that produced no SGRE in its observed lifetime.
Fast CME epoch	A 2-day interval centered on the onset time of the fast CME.
CME cluster	A sequence of CMEs associated with > C-class flares from an AR with waiting times less than a day.
> 3 h SGRE	An SGRE event with a duration > 3 h
l-SGRE	Long-duration SGRE lasting for > 10 h

V_{CME} and a_{CME} as the mean plane-of-sky speed and acceleration measured within the combined field of view of the Large Angle and Spectrometric Coronagraph (LASCO) C2 and C3 coronagraphs. We express F_{CME} on a linear scale where the GOES classes C1.0 – C9.9 correspond to values 1.0 – 9.9, M1.0 – M9.9 to 10.0 – 19.9, and > X1.0 to values above 20.0.

The 'major activity period' of each major AR is estimated as the interval between the first and last observed CMEs associated with > C-class flares. The properties and occurrence of CMEs associated with > C-class flares during the major activity period were quantified for each AR using the parameters listed in Table 2, and their distributions were compared between 'SGRE-producing' and 'SGRE-lacking' AR populations. The distributions of V_{CME} and a_{CME} of fast CMEs associated with > C-class flare in both major AR populations were analyzed and contrasted with those of SGRE-associated CMEs.

After studying the CMEs and their general occurrence characteristics during major activity periods, we explored the temporal clustering of CME events during 'fast CME epochs' in the major activity period of each major AR. We define a fast CME epoch as a 2-day interval centered on the fast CME onset time, and a 'CME cluster' as a succession of CMEs associated with > C-class flares from an AR with waiting times less than a day. CME clusters in the major ARs were identified, and their role in making co-temporal fast CMEs SGRE-associated was investigated. A detailed case study was performed on the CME clusters in two very active major ARs that produced multiple long-duration (> 10 h) SGRE (l-SGRE) events, to understand why fast CMEs in some clusters were SGRE-associated.

Table 1 summarizes all important definitions used in this work. Previous studies that explored the extreme flare productivity of certain ARs had used convenient definitions to pick out super active ARs, or 'super ARs'. Super ARs were first defined by Bai (1987) as ARs producing > 4 major flares. Subsequent works refined the definition by adding criteria on photospheric magnetic field complexity, sunspot properties, radio flux, geomagnetic indices, and SEP flux levels, etc., but without focusing on CME-productivity (Tian, Liu, and Wang 2002; Romano and Zuccarello 2007; Chen et al. 2011; Wang et al. 2013). Similarly, the common definition of a CME cluster does not constrain based on the AR source or associ-

Table 2 Various parameters to characterize the strength of each CME event and major activity period in a major AR.

	Parameter	Definition
CME	F_{CME}	Strength of the associated flare on a scale linear with the GOES class (see, Section 2)
	V_{CME}	Sky-plane speed in the LASCO C2 field of view
	a_{CME}	Residual sky-plane acceleration in the LASCO C2 field of view
Major activity period	ΔT_A	Duration of the major activity period
	N_{CME}	No. of CMEs.
	R_{CME}	$N_{CME}/\Delta T_A$.
	$F_{CME,m}$	F_{CME} of the strongest flare.
	$V_{CME,m}$	V_{CME} of the fastest CME.

ated flare strength of each CME, unlike the definition used in this work. Our definitions of a major AR and a CME cluster are therefore distinct and tailored to strong CME-productive ARs and clustering of energetic events within them, which is relevant for SGRE production.

3. Results and Discussion

We identified 76 major ARs between 2011 and 2019. All >3 h SGRE events in the cycle were associated with 12 major ARs, 5 of which produced the 7 l-SGRE events in the cycle. A table summarizing the properties of the major activity period and associated CMEs for every major AR is provided online.[2] The CME clusters during the major activity periods were also identified in all major ARs, details of which are made available.[3]

This section is divided into four subsections following a top-down approach. Section 3.1 discusses the results at the level of major activity periods and CMEs in general, in the major AR populations. Section 3.2 delves into the properties of fast CME epochs. Section 3.3 discusses the association of fast CME epochs and SGRE events with CME clusters. Finally, Section 3.4 presents a detailed case study exploring the role of CME-CME interactions during CME clusters in SGRE generation.

3.1. Properties of CMEs and Major Activity Periods

Table 2 presents the various parameters of CMEs and major activity periods. A CME is characterized by F_{CME}, V_{CME}, and a_{CME} (see, Section 2). Each major activity period is characterized by its duration (ΔT_A), number of CME events (N_{CME}) and their rate ($R_{CME} = N_{CME}/\Delta T_A$), the maximum observed V_{CME} ($V_{CME,m}$), and the maximum observed F_{CME} ($F_{CME,m}$).

Figure 1 compares the distributions of and Spearman cross-correlations between the various parameters of the major activity period in the SGRE-lacking and SGRE-producing major AR populations. The median values of N_{CME}, R_{CME}, $F_{CME,m}$, and ΔT_A are similar for the two populations, but the median $V_{CME,m}$ and $F_{CME,m}$ are clearly higher (2013 km s^{-1};

[2] https://cdaw.gsfc.nasa.gov/pub/atul/majorARs/MajorAR_CME-flareprops.html

[3] https://cdaw.gsfc.nasa.gov/pub/atul/majorARs

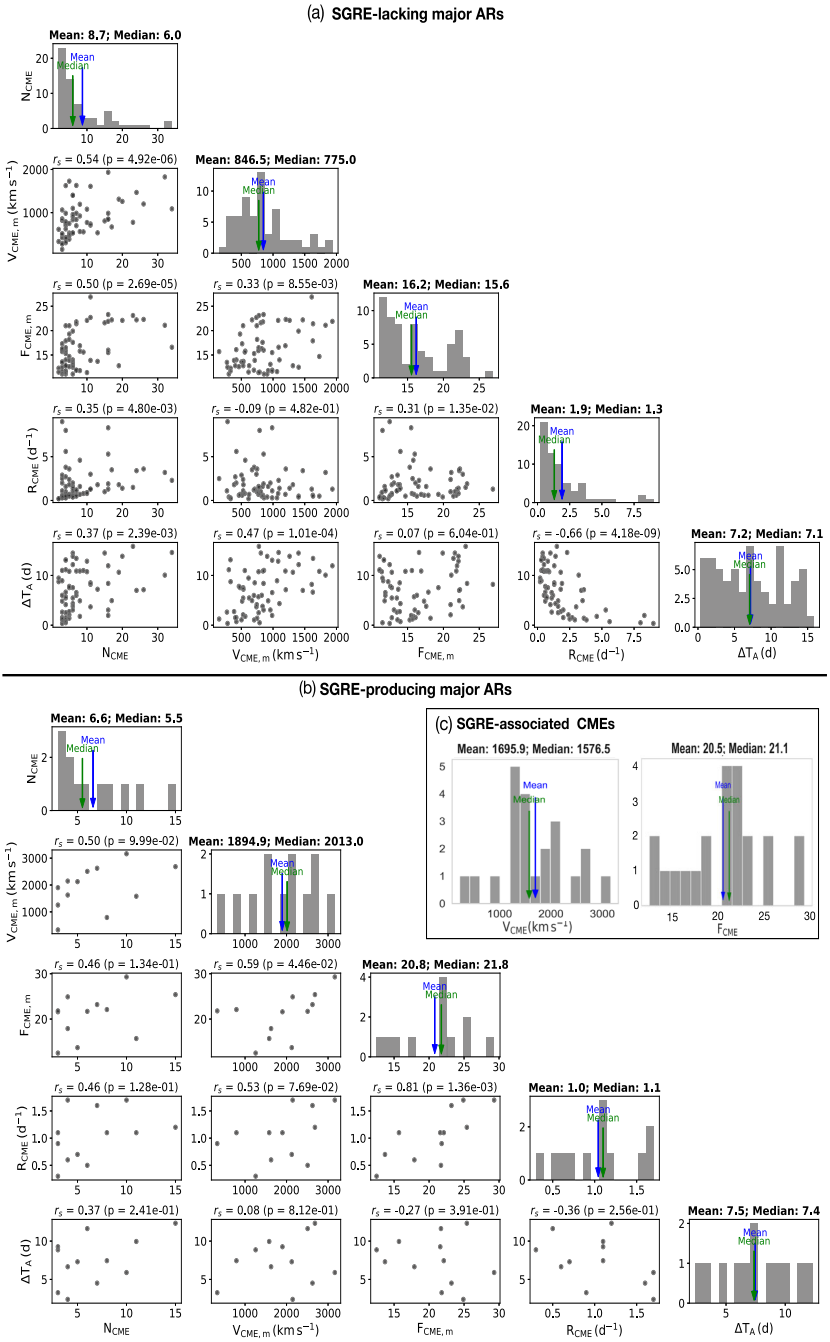

Figure 1 Major activity period characteristics. (a-b): Spearman cross-correlation matrix (r_s: correlation coefficient) with histograms for the various parameters of the major activity period (see Table 2) (c) Histogram of V_{CME} and F_{CME} of SGRE-associated CMEs.

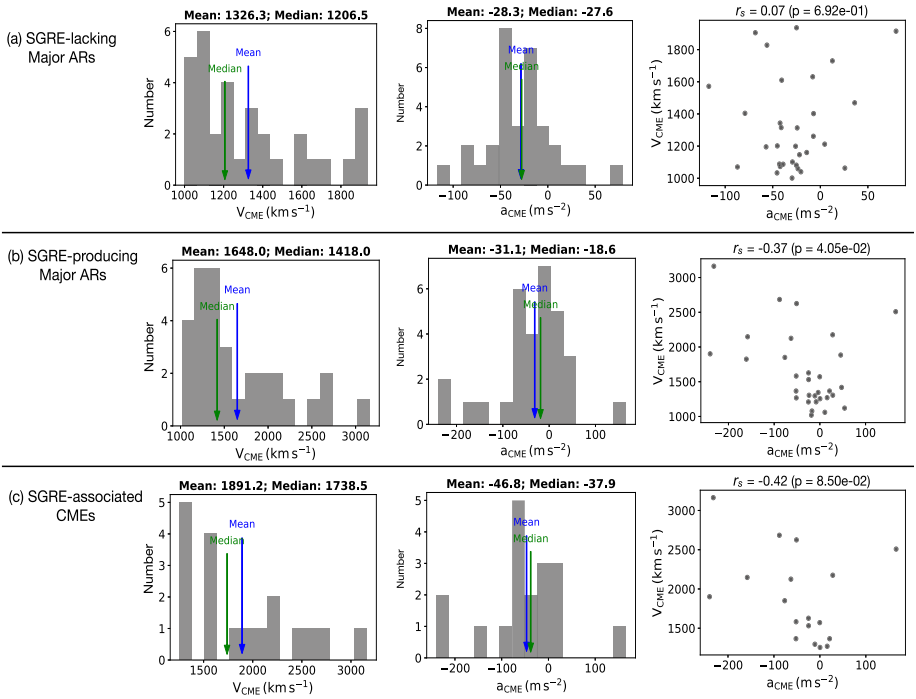

Figure 2 Properties of fast CMEs in SGRE-lacking (a) and SGRE-producing (b) major ARs and those associated with SGRE events (c). Distributions of V_{CME} and a_{CME}, and the Spearman cross-correlation between V_{CME} and a_{CME} are shown.

X1.8) for SGRE-producing ARs, compared to the other (775 km s^{-1}; M5.8). The Spearman correlation coefficient (r_s) between each parameter and the respective p-value is mentioned in Figure 1. The apparent correlation between the R_{CME} and ΔT_A results from the definition of R_{CME}. Meanwhile, based on the p-value and the correlation coefficient (r_s), significant ($p < 0.001$) high correlations ($r_s \gtrsim 0.4$) are found between parameter pairs (ΔT_A, $V_{CME,m}$), (ΔT_A, N_{CME}), ($V_{CME,m}$, N_{CME}), and ($F_{CME,m}$, N_{CME}) for SGRE-lacking major ARs. These parameter pairs remain significantly correlated even after including the SGRE-associated ARs, although the r_s values reduce by 12%, 3%, 20%, and 12%, respectively for each pair. These correlations may simply reflect that longer-lasting ($\approx \Delta T_A$) and more CME-prolific ($\approx N_{CME}$) major activity periods tend to host stronger CMEs that are accompanied by stronger flares. However, despite the similar median values of ΔT_A, and R_{CME}, SGRE-producing ARs are distinguished from the other population by their higher $V_{CME,m}$ and $F_{CME,m}$, highlighting their ability to generate exceptionally fast CMEs associated with stronger flares.

Since CME kinematics clearly play a major role in SGRE generation, we explored the distribution of V_{CME} and a_{CME} for all fast CMEs in major AR populations, compared with the SGRE-associated CMEs (see Figure 2). Of the major AR populations, SGRE-producing ARs generate relatively faster CMEs. The SGRE-associated CMEs form a much faster population of CMEs with very high median residual deceleration (-a_{CME}) within their host ARs. The a_{CME} and V_{CME} show a significant anti-correlation for fast CMEs in SGRE-producing ARs and for SGRE-associated CMEs. This could be because faster CMEs face a high resid-

Table 3 Various parameters to characterize the CME activity in the periods just before (following) each fast CME event. The parameters are defined in the same sense for both periods, with subscripts 'b' and 'f' denoting the periods before and following the fast CME of interest.

Parameter	Definition
$t_{w,b}(t_{w,f})$	Waiting time of the previous (following) CME
$R_{CME,b}(R_{CME,f})$	CME rate in the period before (after) the event onset
$V_{CME,r,b}(V_{CME,r,f})$	Relative sky speed of the preceding (following) CME
$l_{int,b}(l_{int,f})$	Interaction distance parameter with the previous (following) CME

ual deceleration due to a higher solar wind drag force ($\propto V_{CME}^2$) (see, Chen 2011, for an overview). This effect was previously reported for samples of mostly isolated CME events whose evolving structures are well discernible in coronagraphs (Gopalswamy et al. 2000, 2001b,a). However, the lack of a V_{CME} -a_{CME} anti-correlation in the fast CMEs of SGRE-lacking ARs is intriguing, which might be related to the mean ambient conditions during fast CME epochs. The correlation between V_{CME} and a_{CME} is clearly pronounced for very fast (> 1500 km s^{-1}) CMEs, whose dynamics will be relatively less affected by the structures in the propagating medium or near simultaneous eruptions. The following subsection will characterize the fast CME epochs in major ARs, and compare with the SGRE-associated CME epochs.

3.2. Activity of CMEs During Fast CME Epochs

Of the 64 SGRE-lacking major ARs, 17 produced at least one fast CME, and 6 ARs produced at least one very fast CME. Meanwhile, out of the 12 SGRE-producing ARs, 9 hosted very fast CMEs, while one produced a 1200 km s^{-1} CME and two outlier ARs produced < 1000 km s^{-1} CMEs associated with SGRE events lasting for $\lesssim 5$ h.

To characterize each fast CME epoch, we define two sets of parameters for the 1-hour period just before and following the event onset, which are summarized in Table 3. The various parameters include the waiting time for the immediately preceding ($t_{w,b}$) and following ($t_{w,f}$) CMEs, the CME rates (in d^{-1}) before ($R_{CME,b}$) and after ($R_{CME,f}$) the fast CME onset, the relative speed of the immediately preceding ($V_{CME,r,b}$) and following ($V_{CME,r,f}$) CMEs with respect to the fast CME of interest, and the typical interaction distance of the fast CME with the immediately preceding ($l_{int,b}$) and following ($l_{int,f}$) CME. A negative value of $V_{CME,r,b}(V_{CME,r,f})$ implies a relatively slower speed for the preceding (following) CME. The $l_{int,b}$ ($l_{int,f}$) value is computed based on the relative speed and onset time difference of the preceding (following) CME with respect to the fast CME of interest. Since the CMEs considered to compute $l_{int,b}$ ($l_{int,f}$) occur in the same AR, their sky-plane speeds would have very similar projection effects. However, since the details of the CME dynamics are not considered, the estimates of the interaction distance are nominal with lower positive values of $l_{int,b}$ ($l_{int,f}$) indicating higher chances of CME-CME interaction. A negative $l_{int,f}$ ($l_{int,b}$) implies that the CME of interest would not interact with the following (preceding) CME. We remind the reader that only CMEs associated with $>$ C-class flares are considered in this study.

Figures 3 and 4 show the histograms of all parameters in Table 3 characterizing the CME activity during the fast CME epochs of SGRE-producing and SGRE-lacking major ARs. For comparison, statistics for SGRE-associated fast CME epochs are shown separately. Since parameter distributions are generally asymmetric and have outliers, we take the median value of each parameter as its representative estimate. Note that $t_{w,b}$ is negative while $t_{w,f}$ is

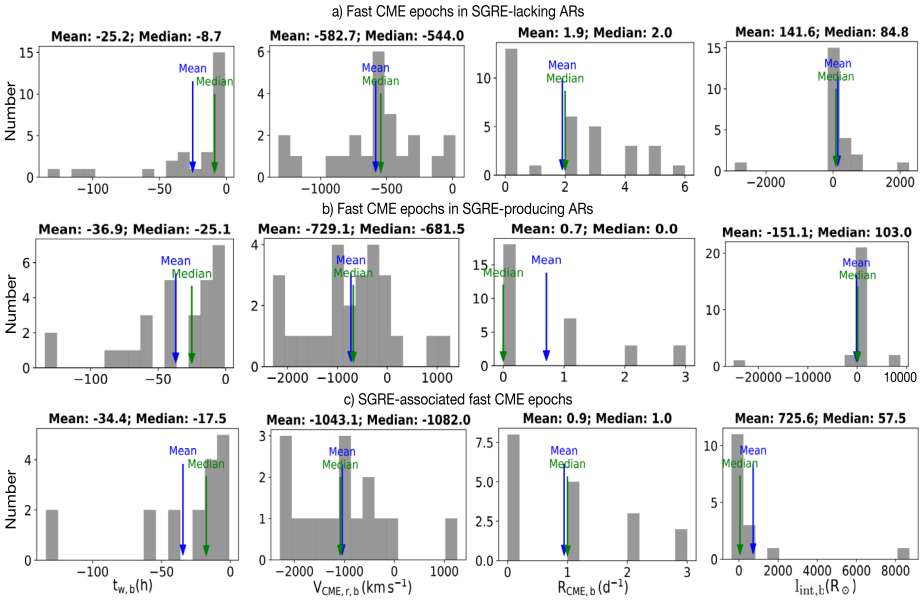

Figure 3 Statistics of the parameters of CME activity in the period just before the fast CME onset within fast CME epochs: (a) in SGRE-lacking major ARs, (b) in SGRE-producing major ARs, and (c) associated with SGRE events.

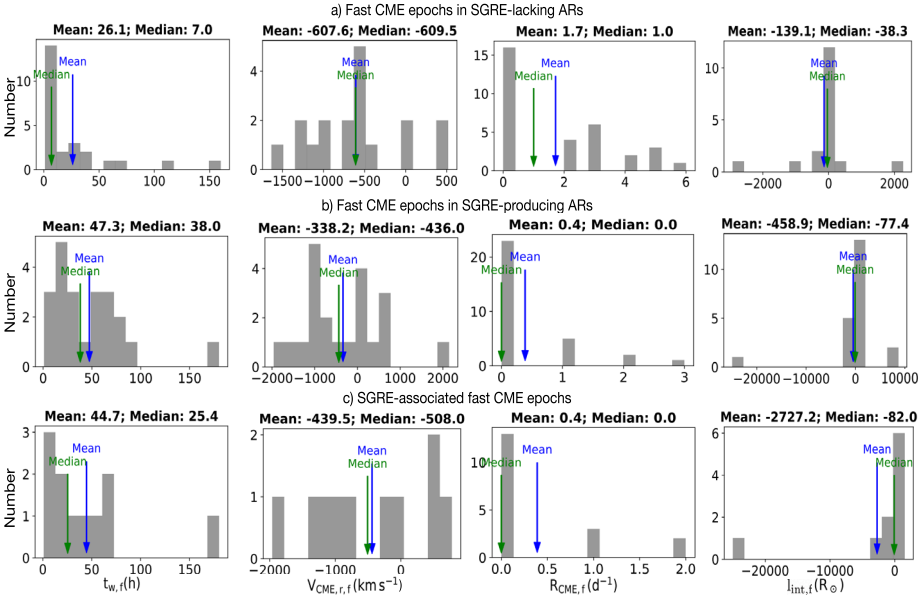

Figure 4 Same as Figure 3, but characterizing the period following the fast CME onset within fast CME epochs.

positive because waiting times are measured from the epoch of the fast CME. We will hence use their absolute values for a comparative analysis of the periods preceding and following the fast CME onset time. The absolute values of $t_{w,b}$ and $t_{w,f}$ are low, while $R_{CME,f}$ and $R_{CME,b}$ are high for SGRE-lacking ARs, compared to SGRE-producing ARs. This could indicate higher chances for CME-CME interactions in SGRE-lacking ARs. However, the median absolute $V_{CME,r,b}$ is higher for SGRE-producing ARs. Since fast CMEs in SGRE-producing ARs are on average faster than those in SGRE-lacking ARs (see, Figure 1), the higher $V_{CME,r,b}$ implies that the interactions of their fast CMEs with the preceding CMEs could be much stronger. The interaction distance is another important parameter because CMEs expand while propagating away from the Sun, causing plasma and magnetic field energy densities to decrease. Hence, CME-CME interactions at lower distances are more energetic with higher particle acceleration potential compared to those occurring at larger distances. The median $l_{int,b}$ of SGRE-producing ARs is higher compared to SGRE-lacking ARs. Meanwhile, negative median values of $l_{int,f}$ for the three populations of fast CME epochs are likely due to the low probability of the occurrence of multiple fast CMEs in short waiting times. This will result in a negative median value for $V_{CME,r,f}$ and in turn $l_{int,f}$.

Next, we investigate CME activity in SGRE-associated CME epochs and compare with the general results for fast CME epochs in the two major AR populations. SGRE-associated CME epochs show significantly lower $l_{int,b}$ and higher $V_{CME,r,b}$ than typical fast CME epochs in major ARs. This suggests higher chances of stronger CME-CME interactions during SGRE-associated CME epochs. In addition, the relatively high median value of $R_{CME,b}$ for SGRE-associated CME epochs compared to a typical fast CME epoch in SGRE-producing ARs suggests that SGRE-associated CME epochs are distinctive periods of high CME activity in their host ARs. To summarize the general CME activity characteristics during fast CME epochs,

1. Fast CME epochs in SGRE-lacking ARs show higher chances of CME-CME interactions.
2. The higher median values for V_{CME} and $V_{CME,r,b}$ for fast CMEs and their epochs respectively in SGRE-producing ARs indicate the chances of relatively stronger CME-CME interactions in these ARs.
3. SGRE-associated CME epochs are periods of higher CME activity in their host ARs, with very high chances of strong CME-CME interactions at low interplanetary space heights.

Though the epochs of SGRE-associated CMEs and fast CMEs in SGRE-lacking ARs show high $R_{CME,b}$, the high $V_{CME,r,b}$ and low $l_{int,b}$ clearly distinguish the former from the latter. A robust investigation of CME-CME interactions during fast CME epochs requires systematic identification and characterization of CME clusters and co-temporal fast CMEs in major ARs.

3.3. CME Clusters in Major ARs

We identified 94 CME clusters across multiple major ARs. The plots of CME occurrences during the major activity period of each major AR with clusters marked are available online, along with the properties of the CMEs and associated flares.[4] Of the identified clusters, 19 found in 16 major ARs had at least one fast CME, and 12 found in 8 ARs had at least one very fast CME. We find that 12 out of 22 (54.5%) SGRE events and 5 out of 7 (71.4%) l-SGRE events occurred in CME clusters. Exploring all these clusters individually in detail

[4] https://cdaw.gsfc.nasa.gov/pub/atul/majorARs/CME_clusters.

Table 4 SGRE events produced by ARs 11429 and 12673.

AR	Event date	Time UT	Dur h	GOES class	V_{CME} km s^{-1}	$V_{CME,sp}$ km s^{-1}	CME cluster
11429	2012-03-05	04:09	4.25	X1.1	1531	1627	Yes
	2012-03-07	**00:24**	**20.47**	**X5.4**	**2684**	**3146**	**Yes**
	2012-03-09	03:53	8.85	M6.3	950	1229	No
	2012-03-10	17:44	11.62	M8.4	1296	1638	No
12673	**2017-09-06**	**12:02**	**18.43**	**X9.3**	**1571**	**1819**	**Yes**
	2017-09-10	16:06	15.18	X8.2	3163	3163	**Yes**

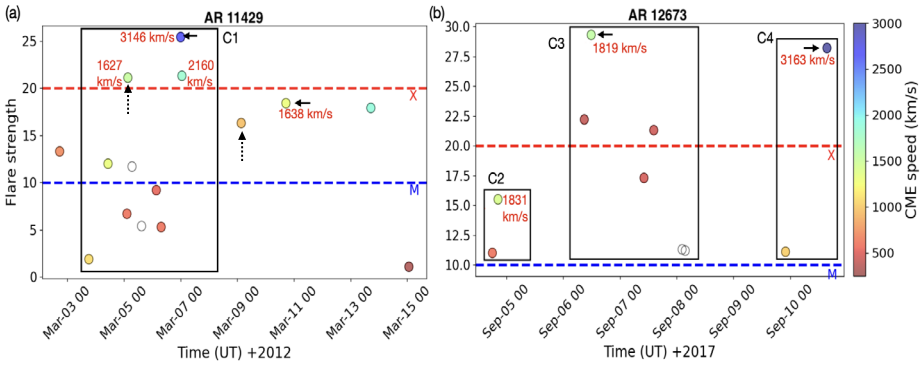

Figure 5 CMEs produced during the major active periods in the selected major ARs. Boxes identify CME clusters (C1 - C4) and horizontal solid arrows mark the l-SGRE-associated CMEs. Vertical dotted arrows mark the other SGRE-associated CMEs. The $V_{CME,sp}$ of all very fast CMEs are mentioned in red text. Label colors provide V_{CME}.

is beyond the scope of this article. Therefore, we resort to a case study of CME clusters in very active major ARs that produced multiple l-SGRE events. ARs 11429 and 12673 are the only such ARs, with some l-SGRE events associated with CME clusters.

3.4. Case Study: CME Clusters in Very Active Major ARs

Table 4 summarizes the properties of the recorded SGRE events in ARs 11429 and 12673 and the associated CMEs. Since V_{CME} is the projected speed in the sky-plane, the true space speed ($V_{CME,sp}$) of every SGRE-associated CME was estimated by fitting a cone CME model (Xie et al. 2006). The columns specify the event date, time, duration, associated flare class, CME speeds, and if the SGRE-associated CME occurred in a cluster. The rows in bold highlight the l-SGRE events that occurred in a cluster. All SGRE-associated CMEs were halo CMEs. Figure 5 shows the various CME clusters during the major activity period of the selected ARs. The solid arrows point to l-SGRE-associated CMEs, when the dotted arrows point to other SGRE-associated CMEs. $V_{CME,sp}$ values of the fast CMEs are shown in red text. Note that cluster C2 in AR 12673 did not produce even a 3-hour-long SGRE, despite having a very fast CME with a $V_{CME,sp}$ similar to that in cluster C3. The following sub-subsections will explore these ARs and clusters in detail.

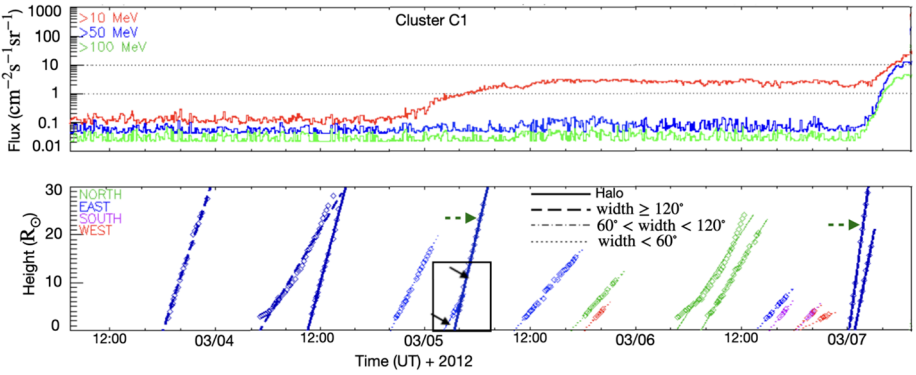

Figure 6 Activity around the period of cluster C1. Top panel shows SEP flux from GOES, while the bottom panel shows the CME height-time measurements marked by diamonds with best-fit lines drawn in different line styles depending on the CME width (see, plot legend). The line and marker colors denote the CME propagation direction. Eastern and northern CMEs are associated with AR 11429. Interacting CMEs from AR 11429 are boxed and marked by black arrows. SGRE-associated CMEs are marked by green dotted arrows.

3.4.1. AR 11429

Cluster C1 produced by the AR lasted from 2012-03-03 18:36 to 2012-03-07 01:30 UT. Two SGRE events that lasted for 20.47 h (l-SGRE) and 4.25 h occurred during the cluster. The AR moved from 83° – 26°E longitude (latitude: 16°N) during the cluster period. Figure 6 shows the SEP flux from GOES in the top panel and the CME height-time plots for all CMEs that occurred during cluster C1, and could be robustly tracked. The data comes from the height-time measurements in the CDAW CME catalog. The height-time data points are colored based on the CME propagation direction, and the slope of the data gives V_{CME}. Green dotted arrows highlight the SGRE-associated CMEs. The box identifies CME-CME interactions, with black arrows pointing at the interacting CMEs. The interaction involving a fast CME of $V_{CME,sp} = 1627\ km\,s^{-1}$ and $a_{CME} = -24.6\ m\,s^{-2}$ was associated with an SGRE that lasted for 4.25 h. The interaction occurred at a short heliocentric distance $< 10\ R_\odot$ with a trailing CME which had a waiting time of −0.78 h and a speed of $-937\ km\,s^{-1}$, relative to the fast CME. These values indicate that the trailing CME was relatively very weak and occurred temporally quite close to the fast CME. Meanwhile, the l-SGRE event on 2012-03-07, associated with a CME of $V_{CME,sp} = 3146\ km\,s^{-1}$, shows no sign of interactions. The two east-directed close-by CMEs on 2012-03-04 are not considered because the earlier of the two events is associated with an AR at N32E87, which is much farther away from AR 11429 (N19E61) that produced the later CME.

Figure 7 explores the epochs of the other two SGRE-associated CMEs from AR 11429, that were not associated with any cluster. The 2012-03-09 03:53 UT event had poor-quality data in LASCO and the Solar TErrestrial RElations Observatory (STEREO) A, making the analysis difficult. However, the CME associated with the l-SGRE event on 2012-03-10 17:44 UT underwent an interaction with a CME from the nearby AR 11430 at a height within 10 $R_\odot$. The waiting time and speed of the trailing CME relative to the fast CME in the interaction are −1.5 h and $-777\ km\,s^{-1}$ respectively. AR 11430 was located ∼ 12° west of AR 11429.

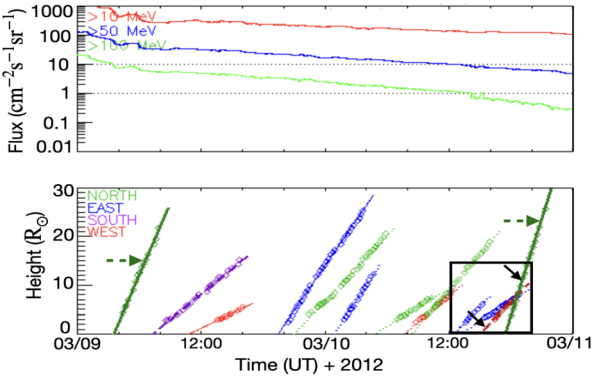

Figure 7 CME activity during SGRE events in AR 11429 (N17W24) unrelated to CME clusters. Figure panels and labels have the same meaning as in Figure 6. The CME associated with the SGRE on 2012-03-10 17:44 UT interacted with an earlier CME from AR 11430 (N18W36).

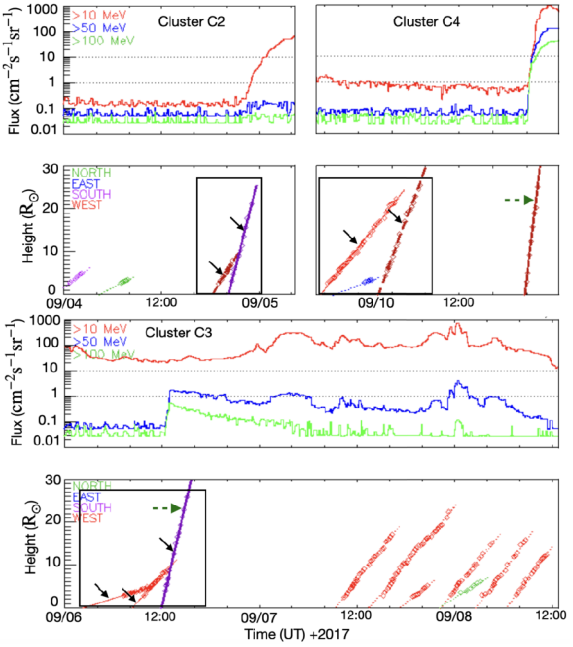

Figure 8 CME clusters in AR 12673. Markers, line styles and labels have the same meaning as in Figure 6.

3.4.2. AR 12673

The AR produced three clusters, C2 – C4. C2 had two CMEs associated with M-class flares on 2017-09-04 at 19:00 and 20:36 UT (see Figure 5b). The latter event was a very fast (1831 km s^{-1}) halo CME. The AR location was S08W11. After a short break, C3 and C4 occurred lasting from 2017-09-06 09:48 to 2017-09-08 04:17 UT and 2017-09-09 23:12 to 2017-09-10 16:00 UT, respectively. The longitude of the AR varied from 11° – 92°W during the period. Figure 8 shows an analysis of the clusters similar to that in Figure 6. We first consider the case of SGRE-associated clusters, C3 and C4. In the case of C3 where a < 2000 km s^{-1} CME produced an l-SGRE, we find clear evidence for multi-step CME interactions involving three CMEs, all within 10 R$_\odot$. The relative CME speeds and waiting times of the two trailing CMEs relative to the fast CME are (-1160 km s^{-1}, -2.5 h) and (-1015 km s^{-1}, -9.6 h). Cluster C4 has a case of CME-CME interaction between

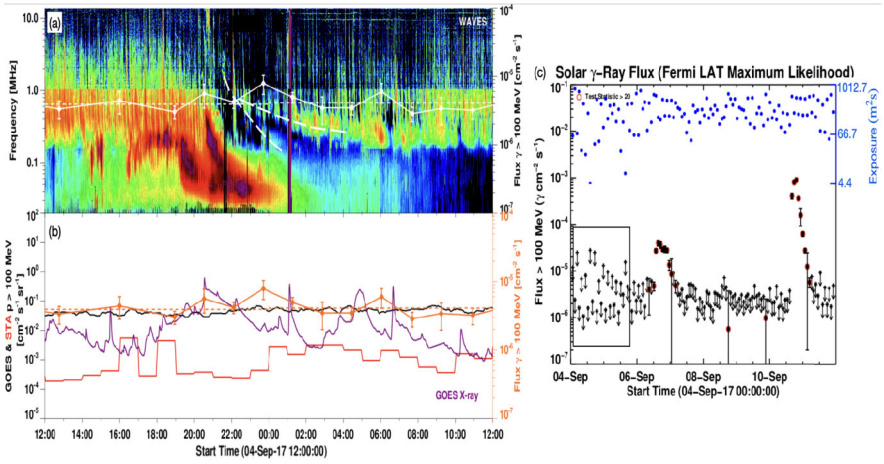

Figure 9 Activity during cluster C2. (a): DH dynamic spectrum showing the type II bursts marked by lines and the spike in γ-ray flux. (b) GOES X-ray flux (purple) and >100 MeV proton fluxes from GOES (black) and STEREO A (red) are shown along with γ-ray flux in orange. (c) The LAT exposures and γ-ray fluxes from the maximum likelihood method are shown. Red points mark the two l-SGRE events that happened in AR 12673. The box region highlights the period of C2.

fast CMEs from AR 12673 marked by the black box. The interaction that occurred at a height above 20 $R_\odot$ did not produce an SGRE. The trailing CME had a speed of about -500 km s^{-1}, with a high waiting time of -5.5 h with respect to the fast CME in the interaction event. Meanwhile, the l-SGRE-associated CME on 2017-09-10 16:06 UT had a $V_{CME,sp}$ of 3163 km s^{-1} with no sign of CME-CME interactions.

Now we consider the case of C2, which did not produce an SGRE despite having a CME-CME interaction involving a fast CME of speed similar to that in C3. The waiting time and speed of the trailing CME were -1.5 h and -821 km s^{-1} respectively, relative to the fast CME in the interaction. The DH dynamic spectrum clearly shows type II radio bursts associated with the CMEs, highlighted by dashed white lines in Figure 9. The overlaid γ-ray light curve shows a minor increase above the mean background level, observed after 2017-09-04 22:00 UT when the CME interaction occurred (see Figure 8). Figure 9c shows the LAT maximum likelihood light curve during the major activity period of AR 12673. The SGRE events during clusters C3 and C4 are highlighted in red circles. The period of C2 is boxed. The noise background during C2 is as high as the flux level of the SGRE event during C3, with very Fermi/LAT exposures. These factors would prevent the robust detection of any SGRE of similar strength as the event during C3, if it had occured during C2.

4. Conclusion

This study investigates the role of CME clustering and CME-CME interactions in >3 h SGRE events. We focus on major ARs, defined as active regions that produced more than one CME-associated major ($>$ M-class) flare during its recorded lifetime. A CME cluster is defined as a series of CMEs with waiting times of less than one day. The study focuses only on CMEs associated with $>$ C-class flares produced by major ARs.

We identified 76 major ARs in Cycle 24 since 2011, using the elaborate database of CMEs, flares, and associated ARs compiled by NASA's CDAW data center. Of these ma-

jor ARs, 12 produced all SGRE events in the FERMI/LAT event lists. The properties of all major ARs are available online. We characterized the major activity period, defined as the period when an AR produced CMEs associated with > C-class flares, of all 76 ARs using various parameters. The parameters include the duration (ΔT_A), the fastest CME speed ($V_{CME,m}$), the strongest flare strength ($F_{CME,m}$), the CME count (N_{CME}) and the average CME rate ($R_{CME} = N_{CME}/\Delta T_A$) associated with the major activity period. Our analysis reveals significant correlations between ($V_{CME,m}$, N_{CME}), ($F_{CME,m}$, N_{CME}), and (ΔT_A, $V_{CME,m}$). This might be a reflection of the fact that longer major activity periods and higher N_{CME} increase the chances for occurrence of faster CMEs. Since SGRE events are closely associated with fast CMEs (> 1000 km s^{-1}), we also examined the distribution of their sky-plane velocity (V_{CME}) and residual acceleration (a_{CME}) within the combined field of view of the LASCO C2 and C3 coronagraphs. We conclude the following about CME activity during the major activity periods of the two major AR populations.

- SGRE-lacking and SGRE-producing ARs have similar ΔT_A and R_{CME}.
- The strongest events in SGRE-producing ARs recorded a much higher median $V_{CME,m}$ (2013 km s^{-1}) and flare class (X1.8), compared to SGRE-lacking ARs (775 km s^{-1}, M5.8).
- Fast CMEs in SGRE-producing ARs have a higher median value of V_{CME} (1418 km s^{-1}) than in SGRE-lacking ARs (1206.5 km s^{-1}).
- SGRE-associated CMEs formed a distinct population with significantly higher median V_{CME} (1738.5 km s^{-1}) and residual deceleration ($a_{CME} = -34.9$ m s^{-2}) within host ARs.

The SGRE-productivity of a major AR is determined by its ability to produce a population of very fast CMEs during its major activity period, independent of the extent of the major activity period or the mean CME rate.

We investigated the clustering and interaction of CMEs during fast CME epochs to explore their potential role in SGRE generation. A fast CME epoch is defined as a 2-hour interval centered on the fast CME onset time. For each fast CME epoch, we estimated the waiting times and relative speed of the immediately preceding and following CMEs. We also computed the CME rates before and after the fast CME onset and interaction distances of the fast CME with the immediately preceding and following CMEs. All fast CME epochs in major ARs were characterized using these parameters. SGRE-associated CME epochs showed very low median values for the interaction distance and CME waiting times, with a high median value for the relative speed with respect to the preceding CME, compared to typical fast CME epochs in major ARs. In addition, SGRE-associated CMEs occurred during periods of enhanced CME rates in their host ARs. Hence, an SGRE-associated CME epoch has the highest probability of a strong CME-CME interaction compared to other fast CME epochs. In addition, we identified 96 CME clusters in all major ARs. Twelve of 22 (54.5%) SGRE events and 5 of 7 (71.4%) long-duration SGRE (l-SGRE) events occurred in CME clusters. Our findings suggest that, like the SGRE-associated fast CMEs, their occurrence epochs also form a distinctive group within their major ARs characterized by higher odds of association to CME clusters and CME-CME interaction.

For a detailed insight, we performed a case study of CME clusters within two very active major ARs, 11429 and 12673, which together hosted four CME clusters and multiple l-SGRE events. All SGRE-associated CMEs in these ARs were halo CMEs with true space speeds ranging from 1627 to 3163 km s^{-1}. AR 12673 was particularly notable, as it had three CME clusters, two of which produced l-SGRE events. We found that all fast CMEs with a speed below 2000 km s^{-1} that were associated with SGRE events had interactions with previous CMEs within distances below 10 $R_\odot$. However, l-SGRE-associated CMEs with speeds > 3000 km s^{-1} did not undergo CME-CME interactions.

These findings emphasize the crucial role of CME clusters and associated CME-CME interactions in the SGRE productivity of fast CMEs with speeds below 2000 km s^{-1}. However, exceptionally fast CMEs ($V_{CME} > 3000$ km s^{-1}) are capable of triggering l-SGRE events independently. We found that the ability of a major AR to produce very fast CMEs in clusters strongly determines its SGRE productivity.

Acknowledgements This work was initiated by the international workshop entitled "Origin of High-Energy Protons Responsible for Late-Phase Pion-Decay Gamma-Ray Continuum from the Sun" supported by the Institute for Space-Earth Environmental Research, Nagoya University. AM and NG are partly supported by NASA's STEREO project, LWS program and the Internal Scientist Funding Model (ISFM). PM, SA, and SY were partially supported by the NSF grant AGS-2043131. We thank the CDAW team for maintaining an up-to-date catalog of solar CMEs detected by the Large Angle and Spectrometric Coronagraph (LASCO) on board the Solar and Heliospheric Observatory (SOHO) mission. The authors also thank the FERMI/LAT team for the γ-ray analysis codes and catalogs.

Author contributions A.M. defined the problem and performed the work. A.M. also wrote the manuscript. P.M. helped A.M. with writing and editing some portions of the manuscript, scientific discussions, and suggestions along the way during the work. N.G. helped in manuscript editing and overall sanity check. The database that was made use of for this work is a personal catalog maintained by S.G. with help from S.Y.. Certain figures in the manuscript derive from the database maintained by S.Y. which was pivotal in the interpretation of results.

Data availability The catalog describing the properties of major active regions (major AR) in Cycle 24 and the directory with relevant plots of important major AR properties can be accessed from this open-access repository, https://cdaw.gsfc.nasa.gov/pub/atul/majorARs/, maintained by NASA CDAW group. All results in the manuscript are based on this database.

Declarations

Competing interests The authors declare no competing interests.

References

Ackermann, M., Allafort, A., Baldini, L., Barbiellini, G., Bastieri, D., Bellazzini, R., Bissaldi, E., Bonino, R., Bottacini, E., Bregeon, J., Bruel, P., Buehler, R., Cameron, R.A., Caragiulo, M., Caraveo, P.A., Cavazzuti, E., Cecchi, C., Charles, E., Ciprini, S., Costanza, F., Cutini, S., D'Ammando, F., de Palma, F., Desiante, R., Digel, S.W., Di Lalla, N., Di Mauro, M., Di Venere, L., Drell, P.S., Favuzzi, C., Fukazawa, Y., Fusco, P., Gargano, F., Giglietto, N., Giordano, F., Giroletti, M., Grenier, I.A., Guillemot, L., Guiriec, S., Jogler, T., Jóhannesson, G., Kashapova, L., Krucker, S., Kuss, M., La Mura, G., Larsson, S., Latronico, L., Li, J., Liu, W., Longo, F., Loparco, F., Lubrano, P., Magill, J.D., Maldera, S., Manfreda, A., Mazziotta, M.N., Mitthumsiri, W., Mizuno, T., Monzani, M.E., Morselli, A., Moskalenko, I.V., Negro, M., Nuss, E., Ohsugi, T., Omodei, N., Orlando, E., Pal'shin, V., Paneque, D., Perkins, J.S., Pesce-Rollins, M., Petrosian, V., Piron, F., Principe, G., Rainò, S., Rando, R., Razzano, M., Reimer, O., Rubio da Costa, F., Sgrò, C., Simone, D., Siskind, E.J., Spada, F., Spandre, G., Spinelli, P., Tajima, H., Thayer, J.B., Torres, D.F., Troja, E., Vianello, G.: 2017, Fermi-LAT observations of high-energy behind-the-limb solar flares. *Astrophys. J.* **835**, 219. DOI. ADS.

Ajello, M., Baldini, L., Bastieri, D., Bellazzini, R., Berretta, A., Bissaldi, E., Blandford, R.D., Bonino, R., Bruel, P., Buson, S., Cameron, R.A., Caputo, R., Cavazzuti, E., Cheung, C.C., Chiaro, G., Costantin, D., Cutini, S., D'Ammando, F., de Palma, F., Desiante, R., Di Lalla, N., Di Venere, L., Dirirsa, F.F., Fegan, S.J., Fukazawa, Y., Funk, S., Fusco, P., Gargano, F., Gasparrini, D., Giordano, F., Giroletti, M., Green, D., Guiriec, S., Hays, E., Hewitt, J.W., Horan, D., Jóhannesson, G., Kovac'evic', M., Kuss, M., Larsson, S., Latronico, L., Li, J., Longo, F., Lovellette, M.N., Lubrano, P., Maldera, S., Manfreda, A., Martí-Devesa, G., Mazziotta, M.N., Mereu, I., Michelson, P.F., Mizuno, T., Monzani, M.E., Morselli, A., Moskalenko, I.V., Negro, M., Omodei, N., Orienti, M., Orlando, E., Paneque, D., Pei, Z., Persic, M., Pesce-Rollins, M., Petrosian, V., Piron, F., Porter, T.A., Principe, G., Racusin, J.L., Rainò, S., Rando, R., Rani, B., Razzano, M., Razzaque, S., Reimer, A., Reimer, O., Serini, D., Sgrò, C., Siskind, E.J., Spandre, G., Spinelli, P., Tak, D., Troja, E., Valverde, J., Wood, K., Zaharijas, G.: 2021, First Fermi-LAT solar flare catalog. *Astrophys. J. Suppl. Ser.* **252**, 13. DOI. ADS.

Akimov, V.V., Belaoussov, A.S., Blokhintsev, I.D., Kalinkin, L.F., Leikov, N.G., Nesterov, V.E., Rodin, V.G., Galper, A.M., Ozerov, Y.V., Popov, A.V., Runtso, M.F., Voronov, S.A., Fradkin, M.I., Topchiev, N.P., Chuikin, E.I., Gerassimov, I.A., Polezshaev, P.N., Tugaenko, V.Y., Gros, M., Bazer-Bachi, A.R., Lavigne, J.-M., Juchniewcz, J.: 1991, Performance of "Gamma-1" telescope in flight. In: *International Cosmic Ray Conference, International Cosmic Ray Conference* **2**, 483. ADS.

Akimov, V.V., Afanasyev, V.G., Belaousov, A.S., Blokhintsev, I.D., Volsenskaya, V.A., Kalinkin, L.F., Leikov, N.G., Nesterov, V.E., Galper, A.M., Voronov, S.A., Zemskov, V.M., Kirillov-Ugryumov, V.G., Lutchkov, B.I., Ozerov, Y.V., Popov, A.V., Rudko, V.A., Runtso, M.F., Chesnokov, V.J., Kurnosova, L.V., Rusakovich, M.A., Topchiev, N.P., Fradkin, M.I., Chuikin, E.I., Tugaenko, V.Y., Tian, T.N., Ishkov, V.N., Gros, M., Grenier, I., Barouch, E., Wallin, P., Baser-Bachi, A.R., Lavigne, J.M., Olive, J.F., Juchniewicz, J.: 1992, Detection of high-energy gamma rays with the Gamma-1 telescope during the solar flares of March 26 and June 15, 1991. *Sov. Astron. Lett.* **18**, 69. ADS.

Atwood, W.B., Abdo, A.A., Ackermann, M., Althouse, W., Anderson, B., Axelsson, M., Baldini, L., Ballet, J., Band, D.L., Barbiellini, G., Bartelt, J., Bastieri, D., Baughman, B.M., Bechtol, K., Bédérède, D., Bellardi, F., Bellazzini, R., Berenji, B., Bignami, G.F., Bisello, D., Bissaldi, E., Blandford, R.D., Bloom, E.D., Bogart, J.R., Bonamente, E., Bonnell, J., Borgland, A.W., Bouvier, A., Bregeon, J., Brez, A., Brigida, M., Bruel, P., Burnett, T.H., Busetto, G., Caliandro, G.A., Cameron, R.A., Caraveo, P.A., Carius, S., Carlson, P., Casandjian, J.M., Cavazzuti, E., Ceccanti, M., Cecchi, C., Charles, E., Chekhtman, A., Cheung, C.C., Chiang, J., Chipaux, R., Cillis, A.N., Ciprini, S., Claus, R., Cohen-Tanugi, J., Condamoor, S., Conrad, J., Corbet, R., Corucci, L., Costamante, L., Cutini, S., Davis, D.S., Decotigny, D., DeKlotz, M., Dermer, C.D., de Angelis, A., Digel, S.W., do Couto e Silva, E., Drell, P.S., Dubois, R., Dumora, D., Edmonds, Y., Fabiani, D., Farnier, C., Favuzzi, C., Flath, D.L., Fleury, P., Focke, W.B., Funk, S., Fusco, P., Gargano, F., Gasparrini, D., Gehrels, N., Gentit, F.-X., Germani, S., Giebels, B., Giglietto, N., Giommi, P., Giordano, F., Glanzman, T., Godfrey, G., Grenier, I.A., Grondin, M.-H., Grove, J.E., Guillemot, L., Guiriec, S., Haller, G., Harding, A.K., Hart, P.A., Hays, E., Healey, S.E., Hirayama, M., Hjalmarsdotter, L., Horn, R., Hughes, R.E., Jóhannesson, G., Johansson, G., Johnson, A.S., Johnson, R.P., Johnson, T.J., Johnson, W.N., Kamae, T., Katagiri, H., Kataoka, J., Kavelaars, A., Kawai, N., Kelly, H., Kerr, M., Klamra, W., Knödlseder, J., Kocian, M.L., Komin, N., Kuehn, F., Kuss, M., Landriu, D., Latronico, L., Lee, B., Lee, S.-H., Lemoine-Goumard, M., Lionetto, A.M., Longo, F., Loparco, F., Lott, B., Lovellette, M.N., Lubrano, P., Madejski, G.M., Makeev, A., Marangelli, B., Massai, M.M., Mazziotta, M.N., McEnery, J.E., Menon, N., Meurer, C., Michelson, P.F., Minuti, M., Mirizzi, N., Mitthumsiri, W., Mizuno, T., Moiseev, A.A., Monte, C., Monzani, M.E., Moretti, E., Morselli, A., Moskalenko, I.V., Murgia, S., Nakamori, T., Nishino, S., Nolan, P.L., Norris, J.P., Nuss, E., Ohno, M., Ohsugi, T., Omodei, N., Orlando, E., Ormes, J.F., Paccagnella, A., Paneque, D., Panetta, J.H., Parent, D., Pearce, M., Pepe, M., Perazzo, A., Pesce-Rollins, M., Picozza, P., Pieri, L., Pinchera, M., Piron, F., Porter, T.A., Poupard, L., Rainò, S., Rando, R., Rapposelli, E., Razzano, M., Reimer, A., Reimer, O., Reposeur, T., Reyes, L.C., Ritz, S., Rochester, L.S., Rodriguez, A.Y., Romani, R.W., Roth, M., Russell, J.J., Ryde, F., Sabatini, S., Sadrozinski, H.F.-W., Sanchez, D., Sander, A., Sapozhnikov, L., Parkinson, P.M.S., Scargle, J.D., Schalk, T.L., Scolieri, G.: 2009, The large area telescope on the Fermi gamma-ray space telescope mission. *Astrophys. J.* **697**, 1071. DOI. ADS.

Bai, T.: 1987, Distribution of flares on the sun: superactive regions and active zones of 1980–1985. *Astrophys. J.* **314**, 795. DOI. ADS.

Chen, P.F.: 2011, Coronal mass ejections: models and their observational basis. *Living Rev. Sol. Phys.* **8**, 1. DOI. ADS.

Chen, A.Q., Wang, J.X., Li, J.W., Feynman, J., Zhang, J.: 2011, Statistical properties of superactive regions during solar cycles 19–23. *Astron. Astrophys.* **534**, A47. DOI. ADS.

de Nolfo, G.A., Bruno, A., Ryan, J.M., Dalla, S., Giacalone, J., Richardson, I.G., Christian, E.R., Stochaj, S.J., Bazilevskaya, G.A., Boezio, M., Martucci, M., Mikhailov, V.V., Munini, R.: 2019, Comparing

long-duration gamma-ray flares and high-energy solar energetic particles. *Astrophys. J.* **879**, 90. DOI. ADS.

Ding, L.-G., Li, G., Jiang, Y., Le, G.-M., Shen, C.-L., Wang, Y.-M., Chen, Y., Xu, F., Gu, B., Zhang, Y.-N.: 2014, Interaction between two coronal mass ejections in the 2013 may 22 large solar energetic particle event. *Astrophys. J. Lett.* **793**, L35. DOI. ADS.

Forrest, D.J., Chupp, E.L., Ryan, J.M., Cherry, M.L., Gleske, I.U., Reppin, C., Pinkau, K., Rieger, E., Kanbach, G., Kinzer, R.L., Share, G., Johnson, W.N., Kurfess, J.D.: 1980, The gamma ray spectrometer for the solar maximum mission. *Sol. Phys.* **65**, 15. DOI. ADS.

Forrest, D.J., Vestrand, W.T., Chupp, E.L., Rieger, E., Cooper, J.F., Share, G.H.: 1985, Neutral pion production in solar flares. In: Jones, F.C. (ed.) *19th International Cosmic Ray Conference (ICRC19), Volume 4, International Cosmic Ray Conference* **4**, 146. ADS.

Gopalswamy, N., Lara, A., Lepping, R.P., Kaiser, M.L., Berdichevsky, D., St. Cyr, O.C.: 2000, Interplanetary acceleration of coronal mass ejections. *Geophys. Res. Lett.* **27**, 145. DOI. ADS.

Gopalswamy, N., Lara, A., Yashiro, S., Kaiser, M.L., Howard, R.A.: 2001b, Predicting the 1-AU arrival times of coronal mass ejections. *J. Geophys. Res.* **106**, 29207. DOI. ADS.

Gopalswamy, N., Yashiro, S., Kaiser, M.L., Howard, R.A., Bougeret, J.-L.: 2001a, Characteristics of coronal mass ejections associated with long-wavelength type II radio bursts. *J. Geophys. Res.* **106**, 29219. DOI. ADS.

Gopalswamy, N., Yashiro, S., Kaiser, M.L., Howard, R.A., Bougeret, J.-L.: 2001c, Radio signatures of coronal mass ejection interaction: coronal mass ejection cannibalism? *Astrophys. J. Lett.* **548**, L91. DOI. ADS.

Gopalswamy, N., Yashiro, S., Krucker, S., Stenborg, G., Howard, R.A.: 2004, Intensity variation of large solar energetic particle events associated with coronal mass ejections. *J. Geophys. Res. Space Phys.* **109**, A12105. DOI. ADS.

Gopalswamy, N., Yashiro, S., Michalek, G., Stenborg, G., Vourlidas, A., Freeland, S., Howard, R.: 2009, The SOHO/LASCO CME catalog. *Earth Moon Planets* **104**, 295. DOI. ADS.

Gopalswamy, N., Mäkelä, P., Yashiro, S., Lara, A., Xie, H., Akiyama, S., MacDowall, R.J.: 2018b, Interplanetary type II radio bursts from Wind/WAVES and sustained gamma-ray emission from Fermi/LAT: evidence for shock source. *Astrophys. J. Lett.* **868**, L19. DOI. ADS.

Gopalswamy, N., Yashiro, S., Mäkelä, P., Xie, H., Akiyama, S., Monstein, C.: 2018a, Extreme kinematics of the 2017 September 10 solar eruption and the spectral characteristics of the associated energetic particles. *Astrophys. J. Lett.* **863**, L39. DOI. ADS.

Gopalswamy, N., Mäkelä, P., Yashiro, S., Lara, A., Akiyama, S., Xie, H.: 2019, On the shock source of sustained gamma-ray emission from the sun. *J. Phys. Conf. Ser.* **1332**, IOP, 012004. DOI. ADS.

Gopalswamy, N., Mäkelä, P., Yashiro, S., Akiyama, S., Xie, H., Thakur, N.: 2020, Source of energetic protons in the 2014 September 1 sustained gamma-ray emission event. *Sol. Phys.* **295**, 18. DOI. ADS.

Gopalswamy, N., Michałek, G., Yashiro, S., Mäkelä, P., Akiyama, S., Xie, H., Vourlidas, A.: 2024, The SOHO LASCO CME Catalog – Version 2. arXiv e-prints, arXiv. DOI. ADS.

Hudson, H.S.: 2018, The relationship between long-duration gamma-ray flares and solar cosmic rays. In: Foullon, C., Malandraki, O.E. (eds.) *Space Weather of the Heliosphere: Processes and Forecasts*, *IAU Symposium* **335**, 49. DOI. ADS.

Kahler, S.W., Cliver, E.W., Kazachenko, M.: 2018, Magnetic flux reconnection in flaring active regions with sustained gamma-ray emission. *Astrophys. J.* **868**, 81. DOI. ADS.

Kanbach, G., Bertsch, D.L., Fichtel, C.E., Hartman, R.C., Hunter, S.D., Kniffen, D.A., Hughlock, B.W., Favale, A., Hofstadter, R., Hughes, E.B.: 1989, The project EGRET (energetic gamma-ray experiment telescope) on NASA's gamma-ray observatory GRO. *Space Sci. Rev.* **49**, 69. DOI. ADS.

Kanbach, G., Bertsch, D.L., Fichtel, C.E., Hartman, R.C., Hunter, S.D., Kniffen, D.A., Kwok, P.W., Lin, Y.C., Mattox, J.R., Mayer-Hasselwander, H.A.: 1993, Detection of a long-duration solar gamma-ray flare on June 11, 1991 with EGRET on Compton-GRO. *Astron. Astrophys. Suppl. Ser.* **97**, 349. ADS.

Kazachenko, M.D.: 2023, A database of magnetic and thermodynamic properties of confined and eruptive solar flares. *Astrophys. J.* **958**, 104. DOI.

Koehn, G.J., Desai, R.T., Davies, E.E., Forsyth, R.J., Eastwood, J.P., Poedts, S.: 2022, Successive interacting coronal mass ejections: how to create a perfect storm. *Astrophys. J.* **941**, 139. DOI.

Lugaz, N., Temmer, M., Wang, Y., Farrugia, C.J.: 2017, The interaction of successive coronal mass ejections: a review. *Sol. Phys.* **292**, 64. DOI. ADS.

Mäkelä, P., Gopalswamy, N., Akiyama, S., Xie, H., Yashiro, S.: 2023, Speed and acceleration of coronal mass ejections associated with sustained gamma-ray emission events observed by Fermi/LAT. *Astrophys. J.* **954**, 79. DOI. ADS.

Mandzhavidze, N., Ramaty, R.: 1992, Gamma rays from pion decay: evidence for long-term trappings of particles in solar flares. *Astrophys. J. Lett.* **396**, L111. DOI. ADS.

Martínez Oliveros, J.C., Raftery, C.L., Bain, H.M., Liu, Y., Krupar, V., Bale, S., Krucker, S.: 2012, The 2010 August 1 type II burst: a CME-CME interaction and its radio and white-light manifestations. *Astrophys. J.* **748**, 66. DOI. ADS.

Mayank, P., Lotz, S., Vaidya, B., Mishra, W., Chakrabarty, D.: 2024, Study of evolution and geo-effectiveness of coronal mass ejection–coronal mass ejection interactions using magnetohydrodynamic simulations with SWASTi framework. *Astrophys. J.* **976**, 126. DOI. ADS.

Mohan, A., Gopalswamy, N., Raju, H., Akiyama, S.: 2024, Novel scaling laws to derive spatially resolved flare and CME parameters from sun-as-a-star observables. *Astron. Astrophys.* **691**, L8. DOI. ADS.

Murphy, R.J., Dermer, C.D., Ramaty, R.: 1987, High-energy processes in solar flares. *Astrophys. J. Suppl. Ser.* **63**, 721. DOI. ADS.

Pesce-Rollins, M., Omodei, N., Petrosian, V., Liu, W., Rubio da Costa, F., Allafort, A., Chen, Q.: 2015, First detection of &gt100 MeV gamma rays associated with a behind-the-limb solar flare. *Astrophys. J. Lett.* **805**, L15. DOI. ADS.

Pesce-Rollins, M., Omodei, N., Krucker, S., Di Lalla, N., Wang, W., Battaglia, A.F., Warmuth, A., Veronig, A.M., Baldini, L.: 2022, The coupling of an EUV coronal wave and ion acceleration in a Fermi-LAT behind-the-limb solar flare. *Astrophys. J.* **929**, 172. DOI. ADS.

Pevtsov, A.A., Fisher, G.H., Acton, L.W., Longcope, D.W., Johns-Krull, C.M., Kankelborg, C.C., Metcalf, T.R.: 2003, The relationship between X-ray radiance and magnetic flux. *Astrophys. J.* **598**, 1387. DOI. ADS.

Plotnikov, I., Rouillard, A.P., Share, G.H.: 2017, The magnetic connectivity of coronal shocks from behind-the-limb flares to the visible solar surface during γ-ray events. *Astron. Astrophys.* **608**, A43. DOI. ADS.

Pomoell, J., Poedts, S.: 2018, EUHFORIA: European heliospheric forecasting information asset. *J. Space Weather Space Clim.* **8**, A35. DOI. ADS.

Ramaty, R., Mandzhavidze, N.: 1998, Solar Flares: Gamma Rays. arXiv e-prints. Astro. DOI. ADS.

Ramaty, R., Murphy, R.J., Kozlovsky, B., Lingenfelter, R.E.: 1983, Gamma-ray lines and neutrons from solar flares. *Sol. Phys.* **86**, 395. DOI. ADS.

Reiner, M.J., Vourlidas, A., Cyr, O.C.S., Burkepile, J.T., Howard, R.A., Kaiser, M.L., Prestage, N.P., Bougeret, J.-L.: 2003, Constraints on coronal mass ejection dynamics from simultaneous radio and white-light observations. *Astrophys. J.* **590**, 533. DOI. ADS.

Rodríguez Gómez, J.M., Podladchikova, T., Veronig, A., Ruzmaikin, A., Feynman, J., Petrukovich, A.: 2020a, Clustering of fast coronal mass ejections during solar cycles 23 and 24 and the implications for CME-CME interactions. *Astrophys. J.* **899**, 47. DOI. ADS.

Rodríguez Gómez, J.M., Podladchikova, T., Veronig, A., Ruzmaikin, A., Feynman, J., Petrukovich, A.: 2020b, Clustering of fast coronal mass ejections during solar cycles 23 and 24 and the implications for CME-CME interactions. *Astrophys. J.* **899**, 47. DOI. ADS.

Romano, P., Zuccarello, F.: 2007, Photospheric magnetic evolution of super active regions. *Astron. Astrophys.* **474**, 633. DOI. ADS.

Ruzmaikin, A., Feynman, J., Stoev, S.A.: 2011, Distribution and clustering of fast coronal mass ejections. *J. Geophys. Res. Space Phys.* **116**, A04220. DOI. ADS.

Ryan, J.M., Lee, M.A.: 1991, On the transport and acceleration of solar flare particles in a coronal loop. *Astrophys. J.* **368**, 316. DOI. ADS.

Salas-Matamoros, C., Klein, K.-L.: 2015, On the statistical relationship between CME speed and soft X-ray flux and fluence of the associated flare. *Sol. Phys.* **290**, 1337. DOI. ADS.

Share, G.H., Murphy, R.J., White, S.M., Tolbert, A.K., Dennis, B.R., Schwartz, R.A., Smart, D.F., Shea, M.A.: 2018, Characteristics of late-phase $>$100 MeV gamma-ray emission in solar eruptive events. *Astrophys. J.* **869**, 182. DOI. ADS.

Temmer, M., Veronig, A.M., Peinhart, V., Vršnak, B.: 2014, Asymmetry in the CME-CME interaction process for the events from 2011 February 14-15. *Astrophys. J.* **785**, 85. DOI. ADS.

Tian, L., Liu, Y., Wang, J.: 2002, The most violent super-active regions in the 22nd and 23rd cycles. *Sol. Phys.* **209**, 361. DOI. ADS.

Wang, Y., Liu, L., Shen, C., Liu, R., Ye, P., Wang, S.: 2013, Waiting times of quasi-homologous coronal mass ejections from super active regions. *Astrophys. J. Lett.* **763**, L43. DOI. ADS.

Xie, H., Gopalswamy, N., Ofman, L., St. Cyr, O.C., Michalek, G., Lara, A., Yashiro, S.: 2006, Improved input to the empirical coronal mass ejection (CME) driven shock arrival model from CME cone models. *Space Weather* **4**. DOI. https://agupubs.onlinelibrary.wiley.com/doi/abs/10.1029/2006SW000227.

Yashiro, S., Gopalswamy, N.: 2008, Statistical relationship between solar flares and coronal mass ejections. *Proc. Int. Astron. Union* **4**, 233. DOI.

Yashiro, S., Gopalswamy, N., Michalek, G., St. Cyr, O.C., Plunkett, S.P., Rich, N.B., Howard, R.A.: 2004, A catalog of white light coronal mass ejections observed by the SOHO spacecraft. *J. Geophys. Res.* **109**. DOI. https://agupubs.onlinelibrary.wiley.com/doi/abs/10.1029/2003JA010282.